PCCP

ROYAL SOCIETY OF CHEMISTRY

PAPER

View Article Online
View Journal | View Issue

Cite this: *Phys. Chem. Chem. Phys.*, 2020, **22**, 21031

Adsorption-induced clustering of CO_2 on graphene†

Giulia Magi Meconi[a] and Ronen Zangi *[bc]

Received 29th June 2020,
Accepted 24th August 2020

DOI: 10.1039/d0cp03482g

rsc.li/pccp

Utilization of graphene-based materials for selective carbon dioxide capture has been demonstrated recently as a promising technological approach. In this study we report results from density functional theory calculations and molecular dynamics simulations on the adsorption of CO_2, N_2, and CH_4 gases on a graphene sheet. We calculate adsorption isotherms of ternary and binary mixtures of these gases and reproduce the larger selectivity of CO_2 to graphene relative to the other two gases. Furthermore it is shown that the confinement to two-dimensions, associated with adsorbing the CO_2 gas molecules on the plane of graphene, increases their propensity to form clusters on the surface. Above a critical surface coverage (or partial pressure) of the gas, these CO_2–CO_2 interactions augment the effective adsorption energy to graphene, and, in part, contribute to the high selectivity of carbon dioxide with respect to nitrogen and methane. The origin of the attractive interaction between the CO_2 molecules adsorbed on the surface is of electric quadrupole–quadrupole nature, in which the positively-charged carbon of one molecule interacts with the negatively-charged oxygen of another molecule. The energy of attraction of forming a CO_2 dimer is predicted to be around 5–6 kJ mol^{-1}, much higher than the corresponding values calculated for N_2 and CH_4. We also evaluated the adsorption energies of these gases to a graphene sheet and found that the attractions obtained using the classical force-fields might be over-exaggerated. Nevertheless, even when the magnitudes of these (classical force-field) graphene–gas interactions are scaled-down sufficiently, the tendency of CO_2 molecules to cluster on the surface is still observed.

Introduction

The extensive use of carbon-based fossil fuels has caused a sharp increase in the concentration of CO_2 gas in the atmosphere, and it might be the major reason why the surface temperature of the earth increased by 1.0 °C over the last sixty years.[1] Therefore searching for alternative, and hopefully renewable, energy sources is one of the main goals for environmental protection. Nonetheless, at the current state of development of clean energy, carbon capture and storage (CCS) is considered a vital approach for reducing the CO_2 level in the atmosphere. This application incorporates several technologies to capture CO_2 from power plants, followed by compression, transport and permanent storage. There are different approaches to separate carbon dioxide from the flue gas stream: solvent absorption, membrane separation and physical adsorption. Currently, solvent absorption using aqueous solutions containing amines or ionic liquids is the most common method employed. Their down-side, however, is that these sorbents are expensive and their regeneration is energy-consuming.[2] Conversely, physical adsorption to porous media has been shown to be a promising alternative due to the high accessible surface area and the ease by which the material can be regenerated in cycle operation, such as by Pressure Swing Adsorption (PSA), or Temperature Swing Asorption (TSA).[3–6]

Many efforts have been made to synthesize porous materials that can efficiently adsorb CO_2 gas. These include zeolites, activated-carbons, silica, polymers, metal–organic frameworks (MOFs) and covalent organic frameworks (COFs).[7] Graphene, a two dimensional material composed of a single layer sp^2 hybridized carbon atom network, has aroused great interest in many fields due to its unusual mechanical, electrical, thermal, and optical properties.[8–11] Graphene is also a powerful adsorbent. This is primarily due to its large electron density above and below the graphene plane, which is able to attract external molecules by London dispersion forces.[12,13] In particular, the capacity of graphene to adsorb CO_2 is quite large, much larger than the potentially competing gases N_2 and

[a] *POLYMAT & Department of Applied Chemistry, University of the Basque Country UPV/EHU, Avenida de Tolosa 72, 20018, San Sebastian, Spain*
[b] *POLYMAT & Department of Organic Chemistry I, University of the Basque Country UPV/EHU, Avenida de Tolosa 72, 20018, San Sebastian, Spain. E-mail: r.zangi@ikerbasque.org*
[c] *IKERBASQUE, Basque Foundation for Science, Maria Diaz de Haro 3, 48013 Bilbao, Spain*

† Electronic supplementary information (ESI) available. See DOI: 10.1039/d0cp03482g

CH_4.[14,15] As a consequence, graphene has a wide range of applicabilities as an adsorbent to capture gaseous pollutants.[16–22]

Obviously, understanding the factors that determine the adsorption capacity of different gases to graphene is of key importance when designing new graphene-based adsorbents. All reports in the literature indicate that at normal operating pressures, the adsorption of CO_2 to graphene is of a physical nature (physisorption).[13] Besides adsorption to bare graphene,[12] many quantum mechanical calculations focused on the effect of different functionalization of the graphene sheet on CO_2 adsorption. For example, oxidized (carboxyl, hydroxyl and epoxy groups)[23] and fluorinated[24] graphene, as well as edge-functionalized graphene,[25] were considered. In addition, the effects of the moisture content (adsorbed water) in coal on the CO_2 adsorption capacity[26] and the chemisorption of CO_2 on graphene, *via* the formation of lactone groups at high pressures,[27] were also investigated. These *ab initio* studies normally employ only a small number of adsorbed molecules, and therefore they are often complemented by classical Monte-Carlo[28–31] or molecular dynamics[32–37] simulations able to consider many more gas molecules and to establish equilibrium conditions between the gas and the adsorbed molecules.

In our previous work[38] we performed molecular dynamics simulations to investigate the adsorption of CO_2 gas by several three-dimensional porous graphene–polymer composite systems and to characterize the discrimination with respect to the capture of N_2 and CH_4 gases. We found that bare-graphene displayed the largest capacity to adsorb CO_2, slightly larger even than a polymer containing three amine/amide groups per monomer. In all cases, CO_2 is preferentially bound relative to nitrogen or methane. Visual inspections of the trajectories revealed that above a critical pressure of CO_2 gas, the adsorbed molecules can form clusters of different sizes, a behavior not observed when N_2 and CH_4 are adsorbed at comparable gas pressures. In the current manuscript, we further investigate and characterize the clustering of the adsorbed carbon dioxide molecules using molecular dynamics simulations and density functional theory calculations.

Methods

Molecular dynamics simulations

We performed molecular dynamics (MD) simulations to investigate the extent of clustering between CO_2 molecules adsorbed on a planar graphene sheet. In order to assess the interaction energies between CO_2 and graphene, as well as between the CO_2 molecules themselves, we performed also quantum mechanical calculations. The results were then compared to those exhibited by N_2 and CH_4 gases.

The preparation of the systems for the MD simulations followed similar protocols to those described in our previous work.[38] A rectangular-shape box with dimensions of 24.065 nm, 24.668 nm, and 64.000 nm along the *x*-, *y*-, and *z*-axes was used for the simulations. Two graphene sheets (that do not interact with each other), periodic in the *xy*-plane, were placed at z_1 = 2.0 nm and z_2 = 62.0 nm. Harmonic potentials with a force constant of 1000 kJ mol^{-1} nm^{-2} were applied to restrain the position of the carbon atoms of the graphene sheets to prevent their translation. Periodic boundary conditions were applied in all three directions; however, they effectively acted only along the *x*-, and *y*-axes because the *z*-coordinates of all gas molecules were confined between z_1 and z_2, *i.e.* within the 60 nm 'inner-region' of the two graphene slabs. We conducted simulations with ternary (CO_2 + N_2 + CH_4) as well as with binary (CO_2 + N_2 or CO_2 + CH_4) gas mixtures. The gas mixtures contained equal numbers of molecules of each gas in the system. The composition of the ternary mixture is $N^{\circ}_{CO_2} = N^{\circ}_{N_2} = N^{\circ}_{CH_2} = \frac{1}{3}N^{\circ}_{gas} = 7000$, and that for the binary gas mixture is $N^{\circ}_{CO_2} = N^{\circ}_{N_2/CH_4} = \frac{1}{2}N^{\circ}_{gas} = 7000$.

The molecular dynamics package GROMACS version 4.6.5[39] was employed to perform all computer simulations in the canonical ensemble (*NVT*) with a time step of 2 fs. The simulation box was fixed during the simulations and a constant temperature of 300 K was maintained by the velocity rescaling thermostat[40] with a coupling time of 0.1 ps. Bond stretching and angle bending were modeled by harmonic potentials. The Lennard-Jones (LJ) interactions between unlike atoms were computed using the geometric combination rules of the OPLSAA force-field. All systems were subjected to a relaxation time of 40 ns and an additional 10 ns were used for the data collection.

The TraPPE model[41] was used to represent the carbon dioxide molecule and the three-site model of Murthy *et al.*[42] was utilized to describe the nitrogen molecule. The latter consists of a massless positively-charged virtual-site (MW), symmetrically situated between the two nitrogen atoms. The non-bonded parameters for the CO_2 and N_2 molecules are specified in Table 1 and the bonded parameters in Table 2. Because in the original simulations of the TraPPE model[41] the Lorentz–Berthelot combination rules were used to mix the Lennard Jones parameters, we also utilized these combination rules when calculating the interactions between the CO_2 molecules. A methane molecule was represented by the OPLSAA force-field.[46] The validation of the force-fields of these three gases in molecular dynamics simulations is reported in our previous study.[38] Nevertheless, the introduction of a positively-charged virtual-site (MW) at the center of the N_2 molecule resulted in an unexpected energy-minimized (steepest descent algorithm) structure for the dimer configuration in which one molecule is perpendicular to the other instead of parallel as

Table 1 The non-bonded parameters for the models of carbon dioxide and nitrogen gas molecules

	q [e]	σ [nm]	ε [kJ mol^{-1}]
C (CO_2)	+0.70	0.280	0.224
O (CO_2)	−0.35	0.305	0.657
N (N_2)	−0.482	0.3318	0.303
MW (N_2)	+0.964	0.0000	0.000

Table 2 The bonded parameters (bond length (b), angle (θ), and the corresponding force constants) for the models of carbon dioxide and nitrogen gas molecules

	b [nm]	K_b [kJ mol^{-1} nm^{-2}]	θ [°]	K_θ [kJ (mol^{-1} rad^{-2})]
C–O	0.116[43]	476 976[43]	180[44]	1236[44]
N–N	0.1098[42]	138 570[45]	—	—

obtained by density functional theory (DFT) calculations. Accordingly, the dimerization energy was also unrealistically large. To circumvent this problem, the two-site model for the nitrogen molecule proposed by Chae and Violi[47] was used (see Table S1 for details, ESI†) when we energy-minimized the classical force-field. We chose to represent graphene as a flexible sheet because the inclusion of thermal motions of the carbon atoms better reproduced its experimental realization. This has been demonstrated recently by comparing the amount of gas adsorbed on rigid and flexible graphene sheets against experimental data.[48] Details of the parameters used to model the flexible graphene sheets (thus including bond stretching and angle bending) are described in a previous simulation study.[49] In this case, the LJ parameters of the carbon atoms, σ_{CC} = 0.3851 nm and ε_{CC} = 0.4396 kJ mol^{-1}, were parameterized to mimic single-walled carbon nanotubes.[50]

A gas molecule is considered adsorbed to the graphene sheet if the distance from its center-of-mass to the graphene center-of-mass, along the z-dimension, is smaller than 0.55 nm. This cutoff value captures almost entirely the unimodal distribution of the adsorbed gas next to graphene as indicated by the density profiles along the perpendicular axis (see for example Fig. 6b in our previous study[38]). More specifically this is computed by the condition,

$$\left| z_C - \frac{1}{N_g}\sum_{i=1}^{N_g} z_{gi} \right| \leq 0.55 \text{ nm}, \quad (1)$$

where z_C and z_{gi} are the components along the z-axis of the position of the carbon of CO_2 and the carbon atoms of graphene, respectively, and N_g = 22 736 is the number of carbon atoms of one graphene sheet. We choose to present the adsorbed gas molecules by the two dimensional mass density, $\rho_{2D} = m/A$, where m is the mass of the adsorbed gas and A is the area of the two graphene sheets. Correspondingly, the bulk mass density is calculated by $\rho_{3D} = m/V$, where m and V are the mass and volume of the gas in the bulk phase. Moreover, two adsorbed gas molecules are considered to be bound to each other if their intermolecular distance is smaller than 0.62 nm. Also here, the position of the molecule is determined by its center-of-mass, and thus by the position of the carbon atom for CO_2 and CH_4 and the dummy atom for N_2. The cut-off value of 0.62 nm roughly corresponds to the first minimum of the radial distribution function between the ($CO_2\cdots CO_2$, $N_2\cdots N_2$, and $CH_4\cdots CH_4$) adsorbed gas molecules.

Quantum chemical calculations

All quantum calculations were carried out using the program Gaussian 16.[51] The optimization of the system geometries was performed at the B3LYP[52] DFT level with long-range dispersion corrections DFT-D3 using the Becke–Johnson damping function.[53] We employed the polarized[54] and diffuse[55] function basis set 6-31+G* of George Petersson and coworkers.[56,57] To model a graphene sheet we used either a coronene ($C_{24}H_{12}$) or a circumcircumcoronene ($C_{96}H_{24}$) molecule. Note that in these cases, the carbon atoms at the edge of the molecule are capped by hydrogen atoms. Therefore, in order to minimize the effect of this edge, the centers-of-mass of the adsorbates, CO_2, N_2, and CH_4, were positioned at the center of the polycyclic aromatic hydrocarbon (PAH) surface.

The adsorption energy of a gas molecule, X, on the polycyclic aromatic hydrocarbon molecule was calculated by,

$$E_{ads} = E_{PAH+X} - E_{PAH} - E_X, \quad (2)$$

the dimerization energy in the gas phase by,

$$E_{dimer(gas)} = E_{dimer} - 2E_{monomer}, \quad (3)$$

and the dimerization (n = 2) or trimerization (n = 3) energy of the adsorbed gas molecules by,

$$E_{n\text{-mer(adsorbed)}} = E_{PAH+n\text{-mer}} + (n-1)E_{PAH} - nE_{PAH+monomer}. \quad (4)$$

Results and discussion

When a molecule in the gas phase is adsorbed on a two-dimensional surface, it loses one degree of freedom of the center-of-mass translation and one (if linear) or two (if not linear) degrees of freedom of rotations around axes parallel to the surface. Consider the process in which the adsorbed molecule subsequently associates with another molecule on the surface. In this case, the resulting dimer translates and rotates as a rigid body and loses the degrees of freedom of the two independent particles. However, because the free particles were confined to two-dimensions, the entropy loss is significantly smaller compared to that if the association process took place in unconfined three dimensional space. This means that when the molecules are adsorbed on a surface, a certain degree of clustering might occur even though in the bulk gas phase the association process is not observed at all.

Although the adsorption strength does not directly influence the propensity to cluster on the surface, it nonetheless indirectly affects clustering because a larger energy of adsorption would normally result in a larger coverage area of the molecules on the surface. When the projected area of the molecules on the surface can not be ignored anymore, an increase in adsorption will lead to a smaller available area on which the molecules can translate, and, therefore, further reduces the entropy loss and promotes clustering. Thus we first start with assessing the adsorption strengths of the gases we consider in this study to graphene by DFT calculations and compare them to those obtained by energy minimization of the classical force-fields.

Adsorption energy of CO_2, N_2, and CH_4 on a graphene sheet model

We calculate the energy of adsorption, E_{ads} (eqn (2)), of a single gas molecule on a graphene sheet model by DFT (B3LYP-D/6-31+G*). As a model for graphene we consider coronene ($C_{24}H_{12}$) and circumcircumcoronene ($C_{96}H_{24}$). The gas molecule was initially placed at the center of the surfaces of these aromatic hydrocarbon molecules. The optimized geometries are shown in Fig. 1. It is evident that the linear gas molecules, CO_2 and N_2, are oriented parallel to the plane of the surface. The carbon atom of CO_2 is situated half-way above two covalently-bonded carbon atoms of the surface, and the two oxygen atoms are placed above the centers of two adjacent aromatic rings. The N_2 molecule is also situated approximately above the center of an aromatic ring. For methane, the plane formed by three hydrogen atoms is parallel to, and in contact with, the surface, whereas the fourth hydrogen is perpendicular to, and pointing away from, the surface. Nevertheless, the two graphene models yield slightly different adsorption positionings of CH_4 relative to the PAH surfaces.

In Table 3 we present the adsorption energies of the three gases in the $C_{24}H_{12}$ and $C_{96}H_{24}$ graphene models, together with the corresponding values of adsorption on a periodic graphene surface obtained from energy minimization of the classical force-field. To evaluate the performance we also provide experimental estimations that used graphite as the adsorbent.

As expected, the larger surface, $C_{96}H_{24}$, results in stronger adsorption energies than the smaller surface, $C_{24}H_{12}$, because there are more adsorbent–adsorbate dispersion attractions. The same trend is also observed for the adsorption energies of CO_2 reported in the literature compiled in Table 4. The values obtained from these previous studies are similar to those reported in the current study, albeit utilizing different sizes of PAHs. Nevertheless, the extrapolation to graphene is not so clear because the two values (−18.4 and −23.1 kJ mol^{-1}) shown in Table 4 differ by 4.7 kJ mol^{-1}. Experimentally, the adsorption energy of CO_2 on graphite (instead of graphene) is estimated to be −17.2 kJ mol^{-1}, a value with smaller magnitude than that obtained by the classical force-field. A similar trend is also observed for N_2 and CH_4, that is, the adsorption energies calculated in this work quantum mechanically and empirically (B3LYP-D and CFF in Table 3) as well as those of other DFT methods in the literature (Table 4) are stronger than the experimental estimations of Vidali *et al.*[58] This suggests that the classical force-field for the graphene–gas interactions used in the MD simulations might be slightly exaggerated and scaling by a factor of approximately 0.7 is necessary.

We also repeated the calculations of the adsorption energy per gas molecule at the B3LYP-D/6-31+G* level on the two PAHs, but instead of adsorbing a single molecule we adsorbed a dimer of the gas molecules. The results are shown in Table S2 (ESI†) and indicate that for the larger PAH, $C_{96}H_{24}$, there is hardly any change in the adsorption energy (0.2–0.3 kJ mol^{-1} discrepancies).

Table 3 Adsorption energy of a single molecule of CO_2, N_2, and CH_4 on the surface of $C_{24}H_{12}$ and $C_{96}H_{24}$ (eqn (2)) using the B3LYP-D/6-31+G* level of calculation. We also show results from steepest-descent energy minimization of the classical force-fields (CFF) utilizing a periodic surface to model the graphene sheet. Experimental estimations of the adsorption energies on graphite are provided in the last column (Exp.). All values are given in kJ mol^{-1}

	B3LYP-D ($C_{24}H_{12}$)	B3LYP-D ($C_{96}H_{24}$)	CFF (graphene)	Exp (graphite)[58]
CO_2	−18.4	−21.5	−25.1	−17.2
N_2	−13.8	−15.8	−13.3	−10.0
CH_4	−13.5	−14.9	−16.5	−12.2

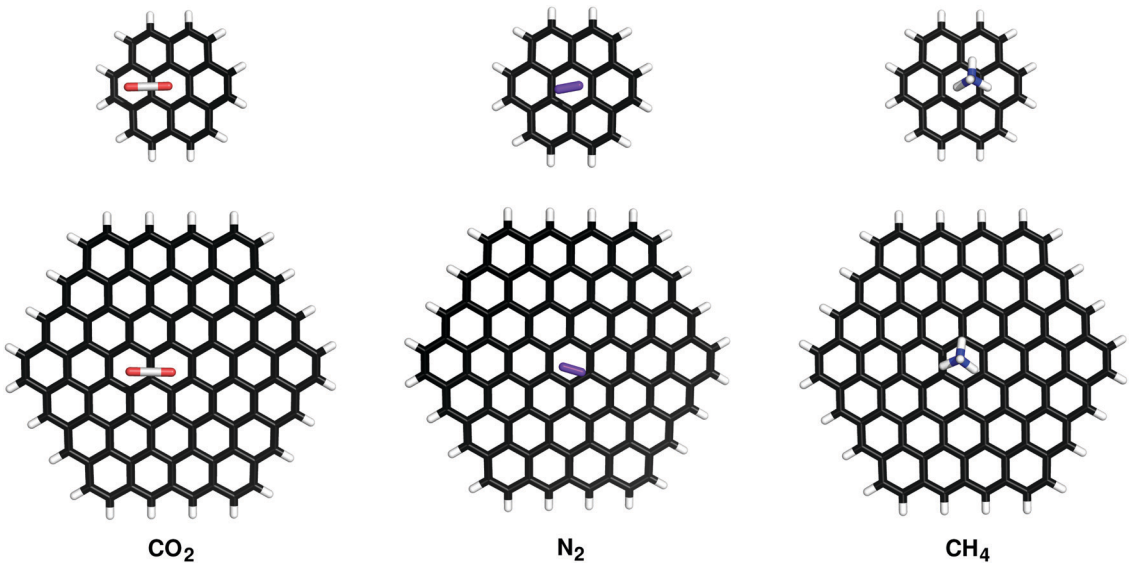

Fig. 1 Top-view of the optimized geometries, obtained at the B3LYP-D/6-31+G* level of theory, of adsorbed CO_2, N_2, and CH_4 on $C_{24}H_{12}$ (top-panel) and $C_{96}H_{24}$ (lower-panel). All bonds are represented by a stick model. The graphene models are colored in black (carbons) and white (hydrogens), carbon dioxide atoms in white (carbon) and red (oxygen), nitrogen molecules in violet, and methane atoms in blue (carbon) and white (hydrogens).

Table 4 Adsorption energies of CO_2, N_2, and CH_4 on a graphene sheet or related polycyclic aromatic hydrocarbons (PAH) reported in the literature. The calculations were performed using different DFT methods and the graphene sheet was modeled by either periodic boundary conditions (PBCs) or by semiPBCs

Adsorbate	Graphene/PAH model	Method	E_{ads} [kJ mol^{-1}]
CO_2	$C_{16}H_{10}$	DFT-D3	−15.6[26]
	$C_{48}H_{18}$	DFT-D3	−17.9[26]
	$C_{54}H_{18}$	wB97X-D	−18.8[12]
	Graphene: PBCs	GGA PBE-D3	−18.4[24]
	Graphene: semiPBCs	DFT+LAP	−23.1[25]
N_2	$C_{54}H_{18}$	wB97X-D	−13.4[12]
CH_4	Graphene: PBCs	GGA PBE-D3	−13.51[24]
	Graphene: semiPBCs	DFT+LAP	−11.1[25]
	$C_{54}H_{18}$	wB97X-D	−17.2[12]

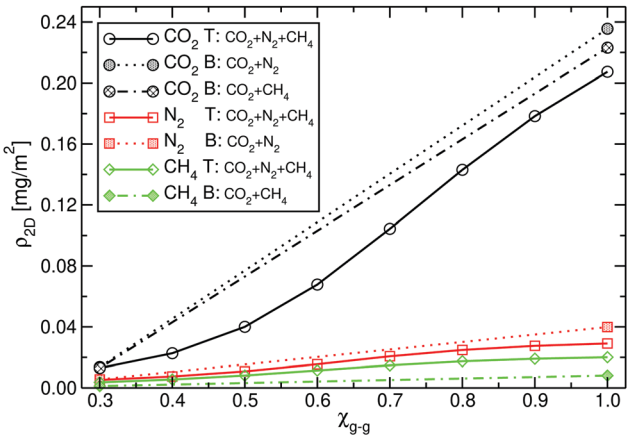

Fig. 2 Adsorption isotherms of CO_2, N_2, and CH_4 gases on graphene at 300 K. The two-dimensional density of the adsorbed gas (averaged over the two graphene surfaces), ρ_{2D}, is plotted as a function of the scaling-factor, χ_{g-g}, of the graphene–gas interaction energy. This factor modifies the strength of the interaction by scaling the LJ parameters ε_{g-g} for all graphene–gas interaction sites. The plot shows data from the ternary, T (solid lines), as well as from the binary, B (dashed or dotted lines), gas mixture systems.

However, for the smaller PAH, $C_{24}H_{12}$, the values are systematically smaller by 1.2–1.4 kJ mol^{-1}, very likely due to unaccounted for dispersion interactions of the dimer when adsorbed on the small surface of $C_{24}H_{12}$.

Scaling the graphene–gas interactions

Given the results above, we conducted simulations of the adsorption of CO_2, N_2, and CH_4 on graphene in which the graphene–gas interactions are scaled down by a factor χ_{g-g} ranging from 1.0 to 0.3 in steps of 0.1 (thus, χ_{g-g} = 1.0 corresponds to the unmodified force-field). Because the graphene carbon atoms do not carry any partial charge, this scaling affects only the depth of the LJ potential well. In Table S3 (ESI†) we specify the value of epsilon between the carbon atom of graphene and any atom of the gases for all values of the scaling factor, χ_{g-g}, considered.

In Fig. 2 we display the adsorption isotherm of each gas (represented by the 2D mass density) as a function of χ_{g-g}. The results were taken from the ternary gas mixture simulations. Nevertheless, the two-end points, χ_{g-g} = 0.3 and 1.0, were simulated also when only two gases were present in the system (binary gas mixtures) and are shown for comparison. Obviously, the amount of gas adsorbed increases for stronger graphene–gas interaction energies. At χ_{g-g} = 0.3 there is negligible adsorption for all gases, whereas at χ_{g-g} = 1.0 CO_2 is adsorbed much stronger than N_2 and CH_4. Correspondingly, the partial pressures of CO_2, N_2 and CH_4 in the bulk phase at χ_{g-g} = 1.0 are 3.1, 6.2, and 9.7 bar, respectively. Note that the curve for CO_2 would have changed to a saturation curve had we chosen to plot the adsorption against the pressure instead of the graphene–gas interaction energy (see Fig. 5a in our previous study[38]). The equilibrium constants of adsorption, $K(x) = \rho_{2D,ad}/\rho_{3D,bulk}$ of the three gases for all graphene–gas interaction strengths are given in Table S4 (ESI†). It is interesting that CO_2 (and to some extent N_2) adsorbs more strongly in the binary mixtures whereas CH_4 adsorbs more strongly in the ternary mixture. As it will be shown below, this can be explained by the fact that adsorbed CO_2 can form stronger attractive interactions with other CO_2 molecules in the binary mixture compared to the ternary mixture. Although CO_2 is observed to have the largest mass density for all values of χ_{g-g}, it is not preferentially bound to graphene for all these scaling factors. To address this point, we evaluate also the preferential adsorption[59] of the gases to graphene.

The preferential adsorption of CO_2 relative to gas X, $\nu'_{CO_2}(x)$, can be defined by,

$$\nu'_{CO_2}(x) = \frac{\theta_{CO_2} N_x}{\theta_x N_{CO_2}}, \quad (5)$$

where θ_i is the number of molecules of gas i adsorbed on graphene and N_i is the corresponding number of molecules in the bulk. This expression then yields a measure of the excess, $\nu'_{CO_2}(x) > 1$, or depleted, $\nu'_{CO_2}(x) < 1$, number of adsorbed CO_2 molecules relative to what would be expected if there was no preference for adsorbing the two gases, *i.e.* a random distribution, $\nu'_{CO_2}(x) = 1$. The procedure of weakening the graphene–gas interaction energy can be exploited when measuring the preferential adsorption of CO_2. It has been shown[60] that if the interaction energy between graphene and gas i (per gas molecule) is u_{g-i} and the standard chemical potential of gas i is μ_i^0, then

$$\ln \nu'_{CO_2}(x) = \beta\left(\mu^0_{CO_2} - \mu^0_x\right) \ln \frac{Z'_{CO_2,ads}}{Z'_{x,ads}} + \beta\left(u_{g-CO_2} - u_{g-x}\right), \quad (6)$$

where $Z'_{i,ads}$ is the single-site molecular partition function, summed over internal energies, of adsorbate i. Thus, a plot of $\ln \nu'_{CO_2}(x)$ as a function of the difference in the adsorption energies of the two gases yields a straight line with a slope of $\beta = 1/k_BT$. These plots of the preferential adsorption of CO_2 with respect to N_2 and CH_4 are shown in Fig. 3a. Linear regression of

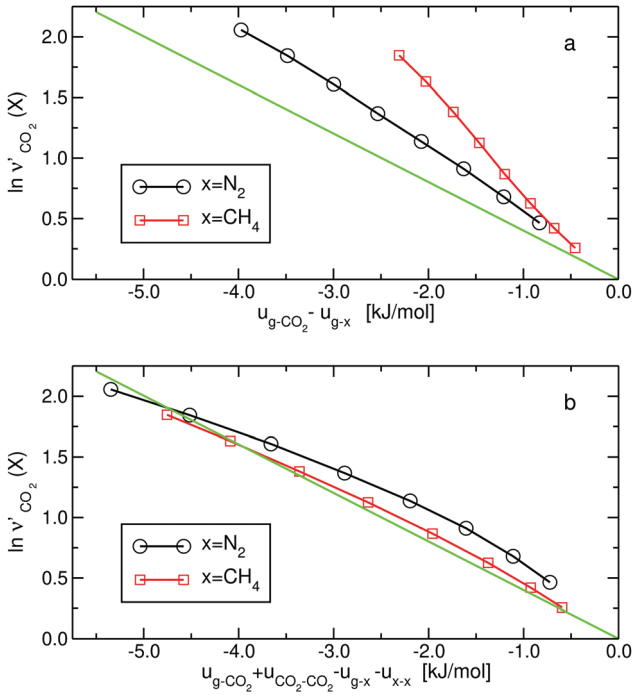

Fig. 3 The preferential adsorption, ν', of CO_2 relative to N_2 and CH_4 gases. In (a) only the difference in the adsorption energies of the gases to graphene is taken into account, whereas in (b) also the difference in the energies of the clustering of the adsorbed CO_2 molecules and that of N_2 or CH_4 are considered. The green line (passing through the origin) corresponds to the theoretical prediction, *i.e.*, it has a slope of $-\beta = -0.4009$ mol kJ^{-1}.

the curves of $\ln \nu'_{CO_2}(N_2)$ and $\ln \nu'_{CO_2}(CH_4)$ gives slopes of -0.51 and -0.88 mol kJ^{-1}, which are quite different from -0.4009 mol kJ^{-1}, the value of β at 300 K. In our previous publication[38] we commented that above a critical partial pressure of CO_2, the adsorbed CO_2 molecules on graphene exhibit a certain degree of clustering. This formation of clusters between the CO_2 molecules increases their effective adsorption energy. Therefore, we calculated these gas–gas interactions of all adsorbed gases (the same calculation but for CO_2 in the bulk gas phase yields negligible values) per molecule, and added their contributions to the difference in the adsorption energies,

$$\ln \nu'_{CO_2}(x) = \beta\left(\mu^0_{CO_2} - \mu^0_x\right) \ln \frac{Z'_{CO_2,ads}}{Z'_{x,ads}} + \beta\left[\left(u_{g-CO_2} + u_{CO_2-CO_2}\right) - \left(u_{g-x} + u_{x-x}\right)\right]. \quad (7)$$

The results are shown in Fig. 3b. Now the linear regression slopes, -0.34 and -0.38 mol kJ^{-1} for $\ln \nu'_{CO_2}(N_2)$ and $\ln \nu'_{CO_2}(CH_4)$, respectively, are much closer to that predicted by eqn (6). Nonetheless, in both cases the actual slopes are smaller than the prediction. This is to be expected because agreement with high accuracy is impeded due to the dependency (even if weak) of the internal partition function of the gases on the degree of clustering. The energies between the adsorbed molecules, u_{x-x}, for $\chi_{g-g} = 0.3$ and 1.0 are specified in

Table 5 The interaction energy (per molecule) between the adsorbate i gas molecules, u_{i-i}, taken from the simulations with the ternary (T) and the binary (B) gas mixtures for $\chi_{g-g} = 0.3$, and 1.0. All values are given in kJ mol^{-1}

	T: CO_2 + N_2 + CH_4		B: CO_2 + N_2		B: CO_2 + CH_4	
	$\chi_{g-g} = 0.3$	$\chi_{g-g} = 1.0$	$\chi_{g-g} = 0.3$	$\chi_{g-g} = 1.0$	$\chi_{g-g} = 0.3$	$\chi_{g-g} = 1.0$
$u_{CO_2-CO_2}$	−0.2	−2.8	−0.2	−3.1	−0.2	−3.0
$u_{N_2-N_2}$	−0.3	−1.4	−0.3	−1.8	—	—
$u_{CH_4-CH_4}$	−0.1	−0.4	—	—	−0.02	−0.1

Table 5. The values obtained from the ternary and binary gas mixtures are very similar. Nevertheless, the slightly stronger interaction of $u_{CO_2-CO_2}$ and $u_{N_2-N_2}$ in the binary gas mixtures and of $u_{CH_4-CH_4}$ in the ternary gas mixture can explain the slightly stronger adsorption observed for these systems in Fig. 2.

Formation of CO_2 clusters on graphene

The improved agreement of the behavior of the preferential adsorption with the theoretical prediction shown in Fig. 3b, relative to that in Fig. 3a, points to the importance of cluster formation of CO_2 molecules to the adsorption thermodynamics. In Table 5 we calculate the number of clusters with size n ($n = 1$ corresponds to monomers, $n = 2$ to dimers, and so on) and show their percentage relative to other clusters with different sizes. In the bulk, the CO_2 molecules are almost

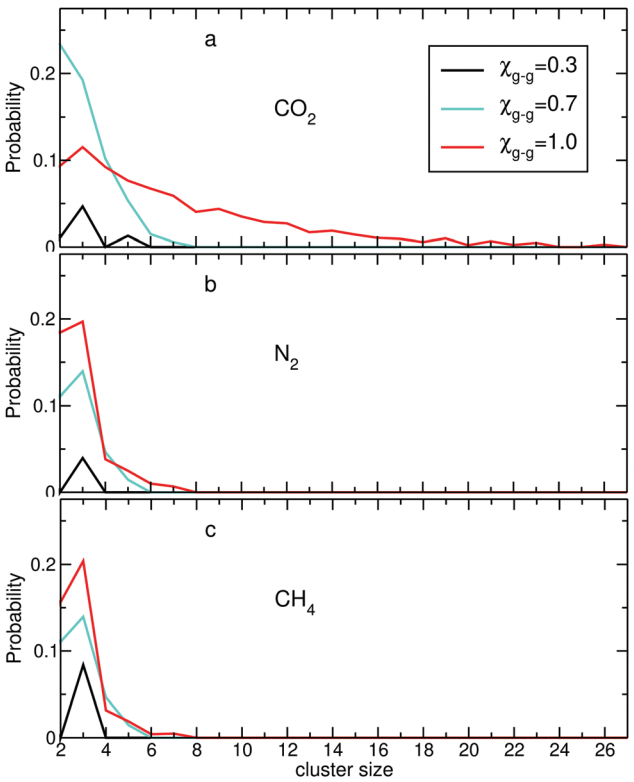

Fig. 4 Normalized distributions of the probability to find a gas molecule in a cluster as a function of the cluster size for (a) CO_2, (b) N_2, and (c) CH_4 for three different scalings of the graphene–gas interaction energy, χ_{g-g}. When available, *i.e.* for $\chi_{g-g} = 0.3$ and 1.0, the results were averaged over the binary and ternary gas mixtures.

Table 6 Percentage of clusters of CO_2 molecules with size n observed in the bulk gas phase as well as adsorbed on graphene, for three different scalings, χ_{g-g}, of the graphene–gas interaction strength. The results are calculated from the simulations of the ternary gas mixture

	Bulk CO_2				Adsorbed CO_2			
	$n = 1$	$n = 2$	$n = 3$	$n \geq 4$	$n = 1$	$n = 2$	$n = 3$	$n \geq 4$
$\chi_{g-g} = 1.0$	99.0	0.5	0.5	0.0	61.7	11.6	8.1	18.6
$\chi_{g-g} = 0.7$	98.1	1.0	0.9	0.0	73.8	14.6	7.2	4.4
$\chi_{g-g} = 0.3$	97.8	1.2	1.0	0.0	96.6	1.3	1.3	0.8

entirely in a monomeric form. The very small percentages of dimers and trimers are not significant; nonetheless, the small increase in their values with decreasing χ_{g-g} is due to larger pressures in the bulk (because fewer CO_2 molecules are adsorbed on the surface). Similar behavior is observed for CO_2 adsorbed on graphene at $\chi_{g-g} = 0.3$. However, for $\chi_{g-g} \geq 0.7$, there is a substantial tendency to form clusters, where dimers and trimers are the most probable cluster sizes. This tendency increases with χ_{g-g} because of larger surface coverages (2D density). In Fig. 4 we provide detailed information about the distribution of clusters with larger sizes. The figure displays the probability to find a gas molecule inside a cluster (composed of molecules of the same gas) as a function of the cluster size, for CO_2, N_2, and CH_4 adsorbed on graphene. Again for the lowest graphene–gas interactions, $\chi_{g-g} = 0.3$, all gases do not cluster substantially. With an increase of χ_{g-g}, the propensity to cluster increases; however, the increase in the association of CO_2 is much larger than that for N_2 or CH_4. For all gases, clusters of sizes three and two are the most probable (the points of the monomers, $n = 1$, are not shown because the magnitudes of their peaks significantly exceed the y-axis scale). At the strongest graphene–gas interaction, $\chi_{g-g} = 1.0$, CO_2 molecules display an appreciable degree of clustering. However as discussed above, this strength of the graphene–CO_2 interaction might be slightly too strong. Nevertheless, even when considering interactions that are weaker by 30% ($\chi_{g-g} = 0.7$) there is still a significant degree of clustering. Note that the quantity calculated in Table 6 to represent the magnitude of clustering is

Table 7 Dimerization and trimerization energies of CO_2, N_2, and CH_4 adsorbed on graphene, $E_{n\text{-mer(adsorbed)}}$ (eqn (4)), calculated at the B3LYP-D/6-31+G* density functional theory level and by energy minimization (steepest descent) using the classical force-field (CFF). For the dimer we also calculated the dimerization energies in the gas phase, $E_{dimer(gas)}$ (eqn (3)). The model for the graphene sheet in the DFT calculations is $C_{96}H_{24}$ and for the classical energy minimization is the same as that used for the MD simulations. All values are given in kJ mol^{-1}

	$E_{dimer(gas)}$		$E_{dimer(adsorbed)}$		$E_{trimer(adsorbed)}$	
	B3LYP-D	CFF	B3LYP-D	CFF	B3LYP-D	CFF
CO_2	−7.1	−5.0	−6.6	−5.0	−12.4	−9.9
N_2	−2.2	−2.1	−1.1	−0.9	−1.6	−2.3
CH_4	−1.8	−1.2	−2.7	−2.0	−5.3	−5.3

different from that calculated in Fig. 4. Whereas the former only considers the number of clusters of each size, the latter weights this number by the size of the cluster. For this reason, the maximum of the distribution of the two quantities can appear at different n. The larger tendency of adsorbed CO_2 molecules to cluster can also be seen in the snapshots displayed in Fig. 5, relative to the weaker tendencies exhibited by N_2 and CH_4 gases shown in Fig. S1 and S2 (ESI†), respectively. It is worth mentioning that the positions of the adsorbed gas molecules obtained from the MD simulations hardly display any commensuration with the graphene structure. This is evidenced by the in-plane radial distribution function between the carbons of adsorbed CO_2 molecules and the carbons of the graphene sheet exhibiting fluctuations with insignificant magnitudes around the value of one (random distribution) as shown in Fig. S3 (ESI†). This is likely due to the large thermal fluctuations at 300 K relative to the interaction energy between the gas atoms and nearest-neighbor carbons of graphene.

In order to assess the cluster formation energy of the classical force-field (CFF) used in the MD simulations, we turn again to DFT calculations. To this end, we calculate the dimerization energy of CO_2, N_2, and CH_4 molecules in a vacuum (eqn (3)) and when adsorbed on graphene (eqn (4)). The results are shown in Table 7. In the gas phase, the

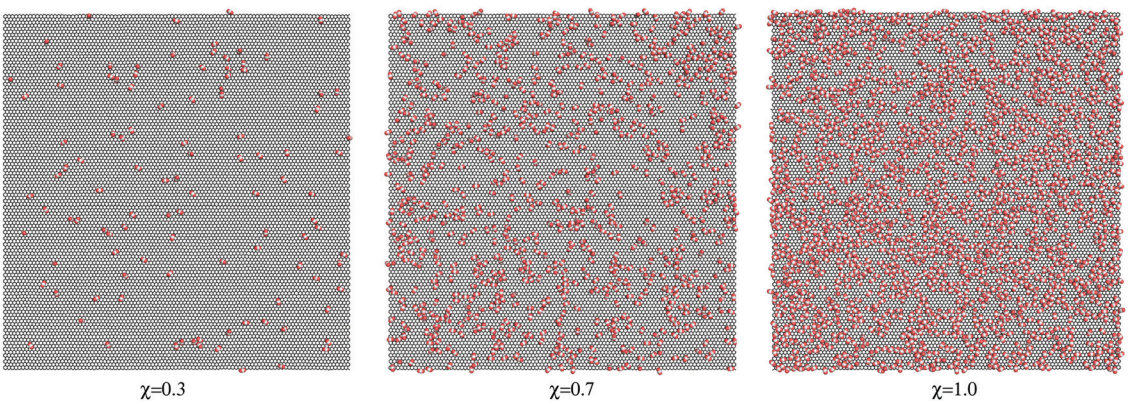

Fig. 5 A top-view projection onto one of the graphene sheets of the adsorbed carbon dioxide molecules for the ternary gas mixture system with graphene–gas interaction strengths of $\chi_{g-g} = 0.3$, 0.7, and 1.0. For clarity, nitrogen and methane molecules are not shown (see Fig. S1 and S2 in the ESI†). Graphene is shown as black sticks and CO_2 molecules as white and red spheres.

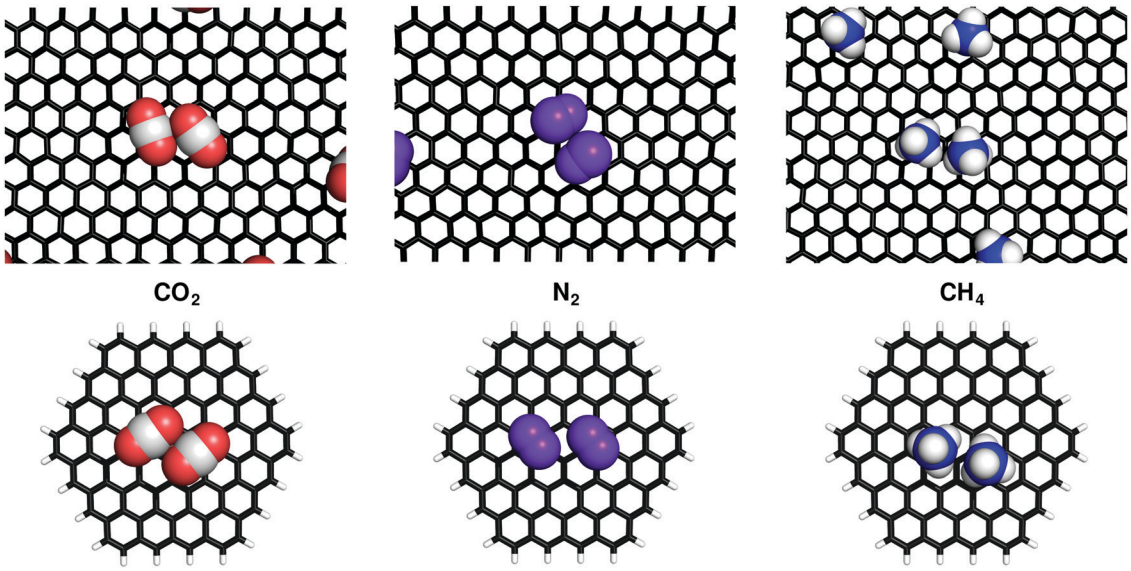

Fig. 6 Structures of the gas dimers obtained from optimization at the B3LYP-D/6-31+G* level adsorbed on $C_{96}H_{24}$ (lower panel), as well as snapshots from the MD simulations adsorbed on graphene (upper panel). Left, middle, and right correspond to CO_2, N_2, and CH_4, respectively.

dimerization energy of the CFF is reproduced quite well for N_2 and CH_4. The largest discrepancy is for CO_2. DFT at the B3LYP-D/6-31+G* level yields a dimerization energy of -7.1 kJ mol^{-1}, whereas energy minimization of the CFF gives -5.0 kJ mol^{-1}. A similar trend is observed for the dimer formation on graphene; the largest discrepancy, 1.6 kJ mol^{-1}, is for CO_2 in which the classical CFF yields a smaller energy of attraction. Thus, if anything, the CFF underestimates the energy to form CO_2 dimers. Furthermore, we would like to stress again that although the dimerization energy is found to be the same in a vacuum and on graphene using the classical force-field, the tendency (*i.e.* change in free energy) to form the dimer is different. This is because the change in the entropy of the dimerization process is different in a 3D vacuum and on the 2D graphene (see Table 6 for the observed clustering propensities in the bulk gas phase and on the graphene surface).

Note that the starting configurations for the energy minimization with the CFF were taken from the optimized structures of the DFT calculations. In all cases, the structures of the dimer (as well as for the trimers desribed below) gas molecules were very similar to the optimized DFT structures. We therefore do not show the energy-minimized structures of the CFF but instead provide snapshots of dimers from the MD simulations and compare them to the DFT optimized structures in Fig. 6. For a CO_2 dimer the DFT-optimized and the MD snapshot configurations are very similar. These structures indicate that the interaction between the two molecules is of a quadrupole–quadrupole nature. The negatively-charged oxygen interacts with the positively-charged carbon and that is why there is an off-set of one atom when two CO_2 molecules approach each other along the axis perpendicular to their principal molecular axes. This interaction is reminiscent of the like-charge attractions between guanidinium cations.[61–63] Taking into account that the experimentally determined[64] electric quadrupole

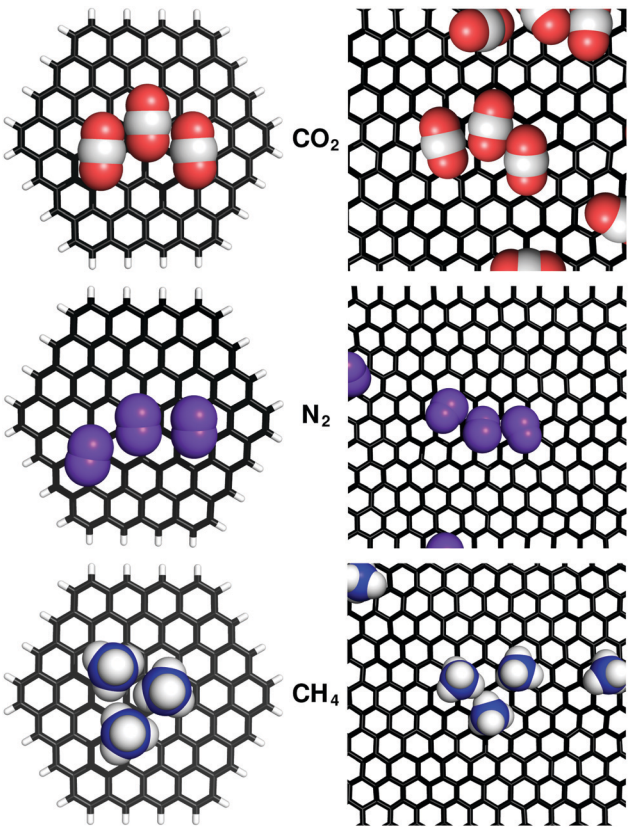

Fig. 7 Left panels: Optimized structures of trimer gas molecules adsorbed on $C_{96}H_{24}$ taken from B3LYP-D/6-31+G* level calculations. Right panels: Snapshots of trimers adsorbed on graphene observed in the MD simulations. Top, middle, and lower panels correspond to CO_2, N_2, and CH_4, respectively.

moment of CO_2 (-13.4×10^{-40} C m^2) is about three times that of N_2 (-4.72×10^{-40} C m^2), similar interactions may also operate in the N_2–N_2 dimer but with a much smaller magnitude.

We also calculated the energy of forming a trimer on graphene (Table 7). As before the only significant difference is for CO_2, in which the B3LYP-D calculation gives a stronger attractive energy (by 2.5 kJ mol^{-1}) than the CFF upon trimer formation. The corresponding comparisons between the DFT-optimized structure and snapshots from the MD simulations are shown in Fig. 7. The quadrupole–quadrupole interaction noted in the CO_2 dimer is clearly present also in the trimer. Note that in the DFT-optimized structure, the third CO_2 is positioned the same as the first molecule, likely to avoid the edge of the surface. In the MD simulations we found this same configuration (as shown in Fig. 7) as well as that in which the third molecule is positioned away from the first molecule, thus forming a diagonal of CO_2 molecules off-set by one atom (not shown).

Conclusions

In this paper we performed computational studies reporting that above a critical value of surface coverage (or gas partial pressure), adsorbed carbon dioxide molecules can form clusters of various sizes on the surface, in which trimers and dimers are the most probable. A similar behavior is not observed for nitrogen and methane gases, nor is it observed for CO_2 in the bulk gas phase, at the temperature and pressures investigated. The molecular origin for the attraction between the CO_2 molecules is quadrupole–quadrupole interactions; the molecules in the clusters are arranged such that atoms on different molecules and with opposite partial charges interact favorably with one another. The magnitude of the attraction in forming a CO_2 dimer, calculated at the B3LYP-D/6-31+G* density functional theory level and by energy minimization of a classical force-field, is on the order of $2k_BT$ at room temperature. This energy of attraction is substantially stronger than the corresponding dimerization energies calculated for nitrogen and methane molecules. Accordingly, the cluster formation of CO_2 molecules was shown to be important to the adsorption thermodynamics, and, in particular, in describing the selectivity of CO_2 with respect to the N_2 and CH_4 gases. It is also likely that the propensity to cluster will influence the mass transport properties of nano-confined fluids.[65] In fact, Sun and Bai[66] found diffusion coefficients of adsorbed CO_2 molecules on graphene, at various pressures, significantly smaller than predicted, whereas the same comparison for CH_4 molecules resulted in a much smaller discrepancy. This can be attributed to an increase in the effective mass of the moving particles due to CO_2 clustering. In addition we calculated by DFT the strength of the adsorption energy between each of the gases and two polyaromatic hydrocarbon molecules as models for a graphene sheet and compared it to that obtained from energy minimization of the classical force-field. The results obtained, as well as the comparison to estimations from experiments, suggest that the classical force-field utilized in this work might overestimate the adsorption energies.

Conflicts of interest

There are no conflicts to declare.

Acknowledgements

This work was supported by a grant from the ministry of economy and competitiveness of the Spanish government, reference number CTQ2016-80886-R. We would like to thank the technical and human support of the computer cluster provided by IZO-SGI SGIker of UPV/EHU and European funding (ERDF and ESF).

References

1 National Centers for Environmental Information, https://www.ncei.noaa.gov, 2018.
2 D. Y. Leung, G. Caramanna and M. M. Maroto-Valer, An overview of current status of carbon dioxide capture and storage technologies, *Renewable Sustainable Energy Rev.*, 2014, **39**, 426–443.
3 R. Dawson, A. I. Cooper and D. Adams, Chemical functionalization strategies for carbon dioxide capture in microporous organic polymers, *Polym. Int.*, 2013, **62**, 345–352.
4 S. Sjostrom and H. Krutka, Evaluation of solid sorbents as a retrofit technology for CO_2 capture, *Fuel*, 2010, **89**, 1298–1306.
5 R. Veneman, Z. Li, J. Hogendoorn, S. Kersten and D. Brilman, Continuous CO_2 capture in a circulating fluidized bed using supported amine sorbents, *Chem. Eng. J.*, 2012, **207–208**, 18–26.
6 B. Lv, B. Guo, Z. Zhou and G. Jing, Mechanisms of CO_2 Capture into Monoethanolamine Solution with Different CO_2 Loading during the Absorption/Desorption Processes, *Environ. Sci. Technol.*, 2015, **49**, 10728–10735.
7 S. Zulfiqar, D. Mantione, O. El Tall, M. I. Sarwar, F. Ruipérez, A. Rothenberger and D. Mecerreyes, Nanoporous amide networks based on tetraphenyladamantane for selective CO_2 capture, *J. Mater. Chem. A*, 2016, **4**, 8190–8197.
8 J. C. Meyer, A. K. Geim, M. I. Katsnelson, K. S. Novoselov, T. J. Booth and S. Roth, The structure of suspended graphene sheets, *Nature*, 2007, **446**, 60–63.
9 K. Scida, P. W. Stege, G. Haby, G. A. Messina and C. D. García, Recent applications of carbon-based nanomaterials in analytical chemistry: Critical review, *Anal. Chim. Acta*, 2011, **691**, 6–17.
10 J. Wang, F. Ma, W. Liang and M. Sun, Electrical properties and applications of graphene, hexagonal boron nitride (h-BN), and graphene/h-BN heterostructures, *Mater. Today Phys.*, 2017, **2**, 6–34.
11 R. K. Matharu, H. Porwal, L. Ciric and M. Edirisinghe, The effect of graphene–poly(methyl methacrylate) fibres on microbial growth, *Interface Focus*, 2018, **8**, 20170058.
12 E. G. Gordeev, M. V. Polynski and V. P. Ananikov, Fast and accurate computational modeling of adsorption on graphene: a dispersion interaction challenge, *Phys. Chem. Chem. Phys.*, 2013, **15**, 18815–18821.
13 M. Pykal, P. Jurečka, F. Karlický and M. Otyepka, Modelling of graphene functionalization, *Phys. Chem. Chem. Phys.*, 2016, **18**, 6351–6372.

14 D. D'Alessandro, B. Smit and J. Long, Carbon dioxide capture: Prospects for new materials, *Angew. Chem., Int. Ed.*, 2010, **49**, 6058–6082.
15 N. Politakos, I. Barbarin, T. Cordero-Lanzac, A. Gonzalez, R. Zangi and R. Tomovska, Reduced Graphene Oxide/Polymer Monolithic Materials for Selective CO_2 Capture, *Polymers*, 2020, **12**, 936.
16 Z. Yang, S. Chabi, Y. Xia and Y. Zhu, Preparation of 3D graphene-based architectures and their applications in supercapacitors, *Proc. Natl. Sci. Mater.*, 2015, **25**, 554–562.
17 Z.-Y. Sui and B.-H. Han, Effect of surface chemistry and textural properties on carbon dioxide uptake in hydrothermally reduced graphene oxide, *Carbon*, 2015, **82**, 590–598.
18 N. Ormategui, A. Veloso, G. P. Leal, S. Rodriguez-Couto and R. Tomovska, Design of Stable and Powerful Nanobiocatalysts, Based on Enzyme Laccase Immobilized on Self-Assembled 3D Graphene/Polymer Composite Hydrogels, *ACS Appl. Mater. Interfaces*, 2015, **7**, 14104–14112.
19 S. Chowdhury and R. Balasubramanian, Holey graphene frameworks for highly selective post-combustion carbon capture, *Sci. Rep.*, 2016, **6**, 21537.
20 S. Gadipelli, Y. Lu, N. T. Skipper, T. Yildirim and Z. Guo, Design of hyperporous graphene networks and their application in solid-amine based carbon capture systems, *J. Mater. Chem. A*, 2017, **5**, 17833–17840.
21 F.-Q. Liu, L.-L. Wang, G.-H. Li, W. Li and C.-Q. Li, Hierarchically Structured Graphene Coupled Microporous Organic Polymers for Superior CO_2 Capture, *ACS Appl. Mater. Interfaces*, 2017, **9**, 33997–34004.
22 L. Ekhlasi, H. Younesi, A. Rashidi and N. Bahramifar, Populus wood biomass-derived graphene for high CO_2 capture at atmospheric pressure and estimated cost of production, *Process Saf. Environ.*, 2018, **113**, 97–108.
23 M. Lalitha and S. Lakshmipathi, Gas adsorption efficacy of graphene sheets functionalised with carboxyl, hydroxyl and epoxy groups in conjunction with Stone–Thrower–Wales (STW) and inverse Stone–Thrower–Wales (ISTW) defects, *Phys. Chem. Chem. Phys.*, 2017, **19**, 30895–30913.
24 D. G. Hwang, E. Jeong and S. G. Lee, Density functional theory study of CH_4 and CO_2 adsorption by fluorinated graphene, *Carbon Lett.*, 2016, **20**, 81–85.
25 B. C. Wood, S. Y. Bhide, D. Dutta, V. S. Kandagal, A. D. Pathak, S. N. Punnathanam, K. Ayappa and S. Narasimhan, Methane and carbon dioxide adsorption on edge-functionalized graphene: a comparative DFT study, *J. Chem. Phys.*, 2012, **137**, 054702.
26 Z. Gao and Y. Ding, DFT study of CO_2 and H_2O co-adsorption on carbon models of coal surface, *J. Mol. Model.*, 2017, **23**, 187.
27 K.-J. Lee and S.-J. Kim, Theoretical investigation of CO_2 adsorption on graphene, *Bull. Korean Chem. Soc.*, 2013, **34**, 3022–3026.
28 L. Joos, J. A. Swisher and B. Smit, Molecular Simulation Study of the Competitive Adsorption of H_2O and CO_2 in Zeolite 13X, *Langmuir*, 2013, **29**, 15936–15942.
29 Y. Liu, X. Zhang, R. M. Blumenthal and X. Cheng, A Common Mode of Recognition for Methylated CpG, *Trends Biochem. Sci.*, 2013, **38**, 177–183.
30 M. Rahimi, J. K. Singh and F. Müller-Plathe, Adsorption and separation of binary and ternary mixtures of SO_2, CO_2 and N_2 by ordered carbon nanotube arrays: grand-canonical Monte Carlo simulation, *Phys. Chem. Chem. Phys.*, 2016, **18**, 4112–4120.
31 H. Wang, Z. Qu, J. Bai and Y. Qiu, Combined grand canonical Monte Carlo and finite volume method simulation method for investigation of direct air capture of low concentration CO_2 by 5A zeolite adsorbent bed, *Int. J. Heat Mass Transfer*, 2018, **126**, 1219–1235.
32 B. Wu and X. Yang, A molecular simulation of interactions between graphene nanosheets and supercritical CO_2, *J. Colloid Interface Sci.*, 2011, **361**, 1–8.
33 S. Jiao and Z. Xu, Selective Gas Diffusion in Graphene Oxides Membranes: A Molecular Dynamics Simulations Study, *ACS Appl. Mater. Interfaces*, 2015, **7**, 9052–9059.
34 W. Li, X. Zheng, Z. Dong, C. Li, W. Wang, Y. Yan and J. Zhang, Molecular Dynamics Simulations of CO_2/N_2 Separation through Two-Dimensional Graphene Oxide Membranes, *J. Phys. Chem. C*, 2016, **120**, 26061–26066.
35 T. T. Trinh, K.-Q. Tran, Q.-V. Bach and D. Q. Trinh, A Molecular Dynamics Simulation Study on Separation Selectivity of CO_2/CH_4 Mixture in Mesoporous Carbons, *Energy Procedia*, 2016, **86**, 144–149.
36 V. S. Kandagal, F. Chen, E. Jónsson, J. M. Pringle and M. Forsyth, Molecular simulation study of CO_2 and N_2 absorption in a phosphonium based organic ionic plastic crystal, *J. Chem. Phys.*, 2017, **147**, 124703.
37 M. Gao, A. J. Misquitta, C. Yang, I. T. Todorov, A. Mutter and M. T. Dove, Molecular dynamics study of CO_2 absorption and desorption in zinc imidazolate frameworks, *Mol. Syst. Des. Eng.*, 2017, **2**, 457–469.
38 G. M. Meconi, R. Tomovska and R. Zangi, Adsorption of CO_2 Gas on Graphene-Polymer Composites, *J. CO_2* Util., 2019, **32**, 92–105.
39 B. Hess, C. Kutzner, D. van der Spoel and E. Lindahl, GROMACS 4: Algorithms for Highly Efficient, Load-Balanced, and Scalable Molecular Simulation, *J. Chem. Theory Comput.*, 2008, **4**, 435–447.
40 G. Bussi, D. Donadio and M. Parrinello, Canonical Sampling through Velocity Rescaling, *J. Chem. Phys.*, 2007, **126**, 014101.
41 J. J. Potoff and J. I. Siepmann, Vapor-liquid equilibria of mixtures containing alkanes, carbon dioxide, and nitrogen, *AIChE J.*, 2001, **47**, 1676–1682.
42 C. Murthy, K. Singer, M. Klein and I. McDonald, Pairwise Additive Effective Potentials for Nitrogen, *Mol. Phys.*, 1980, **41**, 1387–1399.
43 J. Yang, Y. Ren, A.-M. Tian and H. Sun, COMPASS Force Field for 14 Inorganic Molecules, He, Ne, Ar, Kr, Xe, H_2, O_2, N_2, NO, CO, CO_2, NO_2, CS_2, and SO_2, in Liquid Phases, *J. Phys. Chem. B*, 2000, **104**, 4951–4957.
44 J. G. Harris and K. H. Yung, Carbon Dioxide's Liquid-Vapor Coexistence Curve And Critical Properties as Predicted by a Simple Molecular Model, *J. Phys. Chem.*, 1995, **99**, 12021–12024.
45 P. W. Atkins and J. de Paula, *Physical Chemistry*, Oxford University Press, Oxford, UK, 7th edn, 2002.

46 W. L. Jorgensen, D. S. Maxwell and J. Tirado-Rives, Development and Testing of the OPLS All-Atom Force Field on Conformational Energetics and Properties of Organic Liquids, *J. Am. Chem. Soc.*, 1996, **118**, 11225–11236.
47 K. Chae and A. Violi, Mutual diffusion coefficients of heptane isomers in nitrogen: a molecular dynamics study, *J. Chem. Phys.*, 2011, **134**, 044537.
48 J. Vekeman, J. Sánchez-Marín, A. Sánchez de Merás, I. Garcia Cuesta and N. Faginas-Lago, Flexibility in the Graphene Sheet: The Influence on Gas Adsorption from Molecular Dynamics Studies, *J. Phys. Chem. C*, 2019, **123**, 28035–28047.
49 R. Zangi and D. Roccatano, Strings-to-Rings Transition and Antiparallel Dipole Alignment in Two-Dimensional Methanols, *Nano Lett.*, 2016, **16**, 3142–3147.
50 J. H. Walther, R. Jaffe, T. Halicioglu and P. Koumoutsakos, Carbon Nanotubes in Water: Structural Characteristics and Energetics, *J. Phys. Chem. B*, 2001, **105**, 9980–9987.
51 M. J. Frisch, G. W. Trucks, H. B. Schlegel, G. E. Scuseria, M. A. Robb, J. R. Cheeseman, G. Scalmani, V. Barone, G. A. Petersson, H. Nakatsuji, X. Li, M. Caricato, A. V. Marenich, J. Bloino, B. G. Janesko, R. Gomperts, B. Mennucci, H. P. Hratchian, J. V. Ortiz, A. F. Izmaylov, J. L. Sonnenberg, D. Williams-Young, F. Ding, F. Lipparini, F. Egidi, J. Goings, B. Peng, A. Petrone, T. Henderson, D. Ranasinghe, V. G. Zakrzewski, J. Gao, N. Rega, G. Zheng, W. Liang, M. Hada, M. Ehara, K. Toyota, R. Fukuda, J. Hasegawa, M. Ishida, T. Nakajima, Y. Honda, O. Kitao, H. Nakai, T. Vreven, K. Throssell, J. A. Montgomery, Jr., J. E. Peralta, F. Ogliaro, M. J. Bearpark, J. J. Heyd, E. N. Brothers, K. N. Kudin, V. N. Staroverov, T. A. Keith, R. Kobayashi, J. Normand, K. Raghavachari, A. P. Rendell, J. C. Burant, S. S. Iyengar, J. Tomasi, M. Cossi, J. M. Millam, M. Klene, C. Adamo, R. Cammi, J. W. Ochterski, R. L. Martin, K. Morokuma, O. Farkas, J. B. Foresman and D. J. Fox, *Gaussian 16 Revision C.01*, 2016.
52 A. D. Becke, Density-functional thermochemistry. III. The role of exact exchange, *J. Chem. Phys.*, 1993, **98**, 5648–5652.
53 S. Grimme, J. Antony, S. Ehrlich and H. Krieg, A consistent and accurate *ab initio* parametrization of density functional dispersion correction (DFT-D) for the 94 elements H-Pu, *J. Chem. Phys.*, 2010, **132**, 154104.
54 M. J. Frisch, J. A. Pople and J. S. Binkley, Self-consistent molecular orbital methods 25. Supplementary functions for Gaussian basis sets, *J. Chem. Phys.*, 1984, **80**, 3265–3269.
55 T. Clark, J. Chandrasekhar, G. W. Spitznagel and P. V. R. Schleyer, Efficient diffuse function-augmented basis sets for anion calculations. III. The 3-21+ G basis set for first-row elements, Li-F, *J. Comput. Chem.*, 1983, **4**, 294–301.
56 G. Petersson, A. Bennett, T. G. Tensfeldt, M. A. Al-Laham, W. A. Shirley and J. Mantzaris, A complete basis set model chemistry. I. The total energies of closed-shell atoms and hydrides of the first-row elements, *J. Chem. Phys.*, 1988, **89**, 2193–2218.
57 G. Petersson and M. A. Al-Laham, A complete basis set model chemistry. II. Open-shell systems and the total energies of the first-row atoms, *J. Chem. Phys.*, 1991, **94**, 6081–6090.
58 G. Vidali, G. Ihm, H.-Y. Kim and M. W. Cole, Potentials of physical adsorption, *Surf. Sci. Rep.*, 1991, **12**, 135–181.
59 C. Tanford, Extension of the theory of linked functions to incorporate the effects of protein hydration, *J. Mol. Biol.*, 1969, **39**, 539–544.
60 R. Zangi, R. Zhou and B. J. Berne, Urea's Action on Hydrophobic Interactions, *J. Am. Chem. Soc.*, 2009, **131**, 1535–1541.
61 J. Vondrášek, P. E. Mason, J. Heyda, K. D. Collins and P. Jungwirth, The Molecular Origin of Like-Charge Arginine-Arginine Pairing in Water, *J. Phys. Chem. B*, 2009, **113**, 9041–9045.
62 A. Kubíčková, T. Křížek, P. Coufal, E. Wernersson, J. Heyda and P. Jungwirth, Guanidinium Cations Pair with Positively Charged Arginine Side Chains in Water, *J. Phys. Chem. Lett.*, 2011, **2**, 1387–1389.
63 M. Vazdar, F. Uhlig and P. Jungwirth, Like-Charge Ion Pairing in Water: An *Ab Initio* Molecular Dynamics Study of Aqueous Guanidinium Cations, *J. Phys. Chem. Lett.*, 2012, **3**, 2021–2024.
64 C. Graham, J. Pierrus and R. Raab, Measurement of the electric quadrupole moments of CO_2, CO and N_2, *Mol. Phys.*, 1989, **67**, 939–955.
65 C. Sun, R. Zhou, Z. Zhao and B. Bai, Nanoconfined Fluids: What Can We Expect from Them?, *J. Phys. Chem. Lett.*, 2020, **11**, 4678–4692.
66 C. Sun and B. Bai, Gas diffusion on graphene surfaces, *Phys. Chem. Chem. Phys.*, 2017, **19**, 3894–3902.

Electronic Supplementary Material (ESI) for Physical Chemistry Chemical Physics.

Supplementary Information: Adsorption-Induced Clustering of CO_2 on Graphene

Giulia Magi Meconi[1] and Ronen Zangi*[2,3]

[1] *POLYMAT & Department of Applied Chemistry, University of the Basque Country UPV/EHU, Avenida de Tolosa 72, 20018, San Sebastian, Spain*

[2] *POLYMAT & Department of Organic Chemistry I, University of the Basque Country UPV/EHU, Avenida de Tolosa 72, 20018, San Sebastian, Spain*

[3] *IKERBASQUE, Basque Foundation for Science, Maria Diaz de Haro 3, 48013 Bilbao, Spain*

August 12, 2020

*Email: r.zangi@ikerbasque.org

Table S1: Force-field parameters of the two-site model for nitrogen gas molecule proposed by Chae and Violi [J. Chem. Phys. 134, 044537 (2011)].

	q [e]	σ [nm]	ϵ [kJ/mol]	bond [nm]	K_b [kJ/mol·nm^2]
N_2	0.0	0.32973	0.30198	0.1085	1354950.0

Table S2: Adsorption energy, per molecule, of a dimer of CO_2, N_2, and CH_4 on the surface of $C_{24}H_{12}$ and $C_{96}H_{24}$ using the B3LYP-D/6-31+G* level of calculation. More specifically, we calculate the adsorption energy by $E_{ads} = (E_{PAH+X_2} - E_{PAH} - E_{X_2})/2$, where X_2 is the dimer of X. All values are given in kJ/mol.

	$C_{24}H_{12}$	$C_{96}H_{24}$
CO_2	-17.2	-21.3
N_2	-12.6	-15.5
CH_4	-12.1	-15.1

Table S3: The value of the LJ-parameter $\epsilon(C_{gra}–i_{gas})$ between the carbon atoms of graphene and any atom of the three gases, for the different scalings, χ_{g-g}, of the interaction energy between the graphene and the gases. Thus, χ_{g-g}=1.0 corresponds to the unmodified force-field. All values are reported in kJ/mol.

χ_{g-g}	$\epsilon(C_{gra}–C_{CO_2})$	$\epsilon(C_{gra}–O_{CO_2})$	$\epsilon(C_{gra}–N_{N_2})$	$\epsilon(C_{gra}–C_{CH_4})$	$\epsilon(C_{gra}–H_{CH_4})$
1.0	0.31414	0.53735	0.36475	0.34841	0.23490
0.9	0.28273	0.48362	0.32828	0.31357	0.21141
0.8	0.25131	0.42988	0.29180	0.27873	0.18792
0.7	0.21990	0.37615	0.25533	0.24389	0.16443
0.6	0.18849	0.32241	0.21885	0.20905	0.14094
0.5	0.15707	0.26868	0.18238	0.17421	0.11745
0.4	0.12566	0.21494	0.14590	0.13937	0.09396
0.3	0.09424	0.16121	0.10943	0.10452	0.07047

Table S4: Equilibrium constant for adsorption, $K(x)=\rho_{2D,\,ad}/\rho_{3D,\,bulk}$, for x=$CO_2$, N_2, and CH_4. The results are taken from both the ternary (T) and binary (B) gas-mixture simulations for different scalings, χ_{g-g}, of the graphene–gases interaction energies. The values of K are given in nm.

	T: CO_2+N_2+CH_4			**B: CO_2+N_2**		**B: CO_2+CH_4**	
χ_{g-g}	K(CO_2)	K(N_2)	K(CH_4)	K(CO_2)	K(N_2)	K(CO_2)	K(CH_2)
1.0	20.86	2.67	3.29	27.13	3.83	24.16	1.23
0.9	15.88	2.51	3.11	—	—	—	—
0.8	11.18	2.24	2.81	—	—	—	—
0.7	7.19	1.83	2.34	—	—	—	—
0.6	4.20	1.35	1.76	—	—	—	—
0.5	2.30	0.93	1.23	—	—	—	—
0.4	1.25	0.63	0.82	—	—	—	—
0.3	0.70	0.44	0.54	0.73	0.46	0.70	0.18

Table S5: The interaction energy between the same-type gas molecules, u_{x-x}, adsorbed on graphene for the ternary gas mixture simulations at different scalings of the graphene-gas interaction strength, χ_{g-g}. All energies are given in kJ/mol.

χ_{g-g}	$u_{CO_2-CO_2}$	$u_{N_2-N_2}$	$u_{CH_4-CH_4}$
1.0	-2.8	-1.4	-0.4
0.9	-2.4	-1.3	-0.3
0.8	-1.9	-1.2	-0.3
0.7	-1.4	-1.1	-0.2
0.6	-0.9	-0.8	-0.2
0.5	-0.6	-0.6	-0.1
0.4	-0.3	-0.4	-0.1
0.3	-0.2	-0.3	-0.1

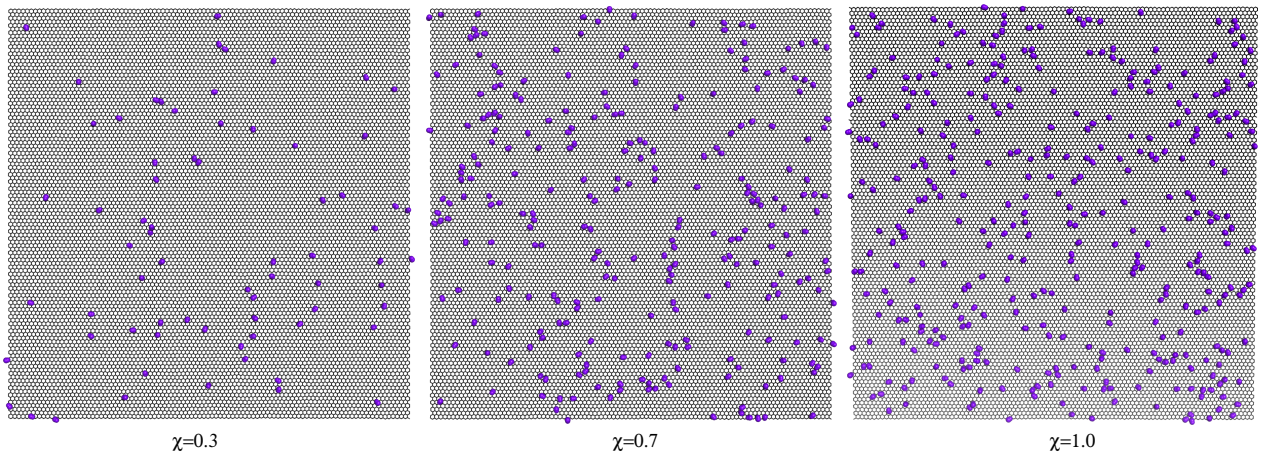

Figure S1: A top-view projection onto one of the graphene sheets of the adsorbed nitrogen molecules for the ternary gas mixture system with graphene-gas interaction strength of χ_{g-g}=0.3, 0.7, and 1.0. For clarity, carbon dioxide and methane molecules are not shown here (see Fig. 5 and Fig. S2). Graphene is shown as black sticks and N_2 molecules as purple spheres.

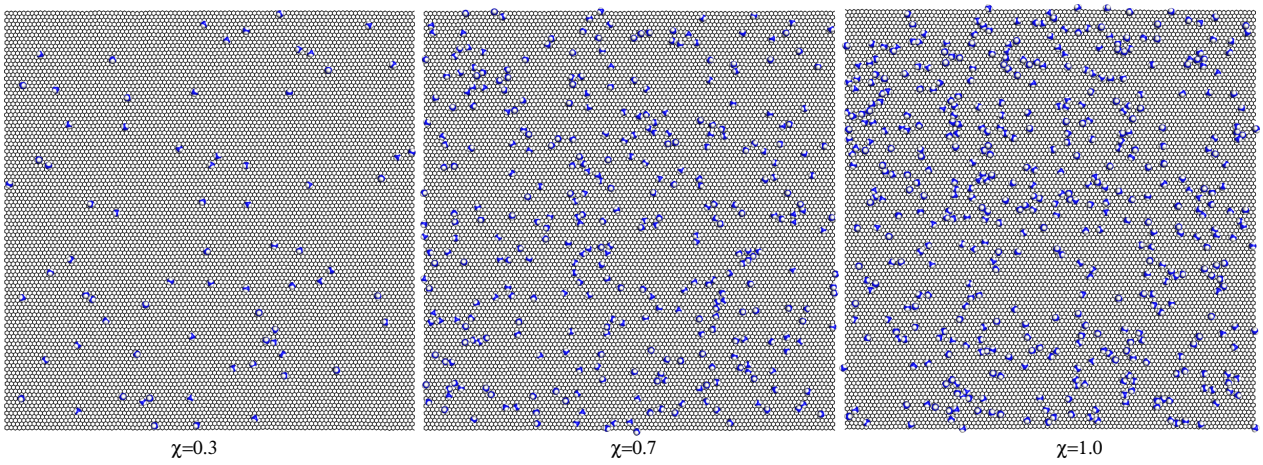

Figure S2: Same as Fig. 5 and Fig. S1 but for the methane molecules.

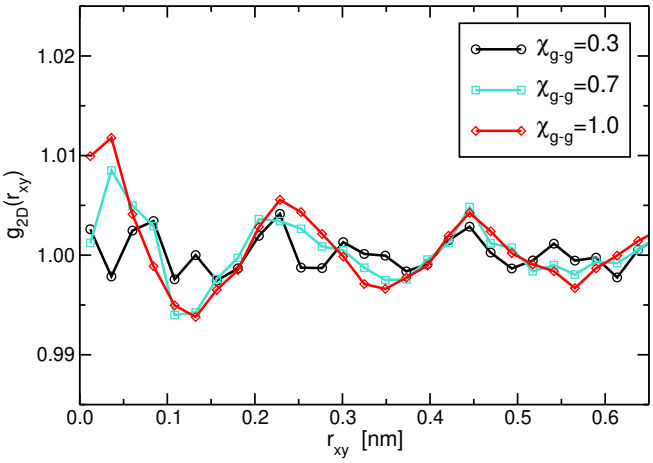

Figure S3: Two-dimensional radial distribution functions, projected on the xy-plane, between the carbon atoms of adsorbed CO_2 molecules and the carbons of the graphene sheet on which the CO_2 molecules are adsorbed, for three different scalings of the graphene-gas interaction energy.